IEEE Access
Multidisciplinary | Rapid Review | Open Access Journal

Received October 7, 2021, accepted October 23, 2021, date of publication October 27, 2021, date of current version November 8, 2021.

Digital Object Identifier 10.1109/ACCESS.2021.3123355

Design, Control and Implementation of Torus-Type Omniorientational Blimp With Tilting Actuators

SEUNG HWAN SONG, (Student Member, IEEE), AND HYOUK RYEOL CHOI, (Fellow, IEEE)
School of Mechanical Engineering, Sungkyunkwan University, Suwon 440746, Republic of Korea

Corresponding author: Hyouk Ryeol Choi (choihyoukryeol@gmail.com)

This research was supported by the MSIT(Ministry of Science and ICT), Korea, under the Grand Information Technology Research Center support program(IITP-2021-2015-0-00742) supervised by the IITP(Institute for Information & communications Technology Planning & Evaluation).

ABSTRACT Buoyancy-aided unmanned aerial vehicle (UAV) has a powerful advantage in terms of flight time and safety, compared to conventional multirotors. However, previously developed platforms showed limited flight maneuverability (i.e. omnidirectional translation) and posture transition (i.e. omniorientational rotation) owing to lack of number of actuators or limit of design specifications. As a solution, this study presents a symmetric torus blimp, which is pierced in the middle of envelope and surrounded by four tiltable actuator. All flight-aid electric parts are located in the center of the hole to match center of buoyancy with center of mass. And four motors mounted along the edge of the hull can be tilted by each linked servo. Owing to symmetric design and sufficient number and allocation of actuators, stable independent omniorientational and omnidirectional motion during flight that standard blimp or multirotors hard to do can be easily performed. This performance can be achieved by simple feedback control algorithm based on aerodynamic model. Also, a novel control allocation based on a fully-actuated system is described for independent orientation and position control. The result of various angle tracking orientation control and stabilization control experiments performed are presented. In addition, omnidirectional control with manual control keeping orientation independently is validated. Finally, narrow space passing and omnidirectional wall interaction results are described to demonstrate the advantages of the specification of this platform.

INDEX TERMS Unmanned aerial vehicle, hellium-filled blimp, buoyancy, tilting actuator, soft drone.

I. INTRODUCTION

In the past decade, multirotor unmanned aerial vehicle (UAV), commonly known as drone, have been extensively researched and are being used in various industries, such as hobby, agriculture, structure, rescue, filming, and delivery [1]–[4]. Simultaneously, problems such as low flight efficiency, safety and noise issues, and underactuated movement are emerging as obstacles in more diverse applications. Lighter-than-air vehicles, such as helium-filled blimps, have been studied as a solution to these problems and have shown new possibilities by performing omnidirectional flight motions and unique missions that conventional drones cannot perform.

The airship, which is the most representative helium-filled blimp, has been studied in a form wherein a rotor is attached to the surface of a balloon and electric parts are contained in a gondola. A typical blimp includes a rotor and gondola attached to the bottom of the aircraft, similar to the aircraft featured in [5]. This shows its indoor applications like aerial filming near crowd [6] with successful maneuvering performance. In contrast, Wan *et al.* demonstrated more stable flight performance through the dynamic modeling of a blimp with three rotors attached to the side and below [7]. Furthermore, Wang *et al.* successfully demonstrated disturbance compensation control of blimps in the form of a rotor attached to a gondola [8]. The previous three studies showed only one-dimensional flight motion owing to the asymmetry of the shapes and the parts attached around the blimp. A torus or spherical shape has been proposed as an alternative that overcomes the limitation of symmetry, and

The associate editor coordinating the review of this manuscript and approving it for publication was Agustin Leobardo Herrera-May.

various actuation mechanisms for flight control have consequently been proposed [9]–[14]. Suefuku *et al.* analyzed the dynamic characteristics of a torus-type blimp through simulations and experiments [9] and demonstrated omnidirectional movement. Song *et al.* presented a new vehicle with a flow control mechanism [10], showing the usability of vehicle advertisements and entertainment near crowds. The previous two studies suggested a new type of torus-shaped blimp model, but there is a limitation with regard to stable attitude control. In contrast, Tao *et al.* presented a unique control model for the swing motion of a spherical blimp with a gondola attached at the bottom, which showed good flight performance [11]. In addition, Festo achieved stable flight motion of a spherical vehicle by attaching numerous rotors around it, thereby successfully demonstrating good flight performance and pick-and-place in various situations [12]. However, there is a dependency between the orientation and position control of the vehicle, and a complex system is required for controlling multiple rotors. Helium-filled vehicle using piezo elements as actuator is a novel concept; this vehicle can safely fly around people [13]. Another spherical drone shows high safety using Coanda effect [14]. In addition, another study used a cube-shape helium-filled vehicle for flight show near people [15]. Helium-filled body robot with two legs is also introduced [16]. Although there have been new use cases, such as aerial show and advertisements, using helium-filled drone, the existing actuation mechanism and control design are inadequate to independent attitude control and position control.

The underactuated quadrotor is generally controlled by a cascaded structure, and inevitably, the orientation control is subordinated to the position control [17]. Consequently, the quadrotor must be unconditionally tilted for movement. A gimbal and a complex control algorithm are required for aerial photography and aerial manipulation, respectively [18]. To solve this problem, fullyactuated systems with various tilting rotor mechanisms have been proposed [19]. Adjusting the location and orientation coordinates of the rotors enable the wrench generation motion of the vehicle to be more capable than that of conventional drones. A fullyactuated system decouples the position and orientation control, resulting in an omnidirectional flight motion. This system is achieved by tilting the rotor frame in arbitrary directions [20]–[23] or by allocating the optimal rotor configurations [24]–[27].

The tilting rotor mechanism mounted on the helium-filled hull achieved both high flight efficiency and dexterous maneuvers performance. Four tetrahedrally arranged actuation units mounted on a spherical hull made by Burri *et al.* [28] exhibited redundant control in 6 degrees of freedom (DoF) of motion and aerial filming above the crowd using a camera module mounted on the hull. They presented tetrahedral solution is the most suitable for omnidirectional motion and made this with 2.7 m diameter spherical blimp. Similarly, Malek *et al.* developed a large size hybrid airship vehicle using four propellers arranged as a quadcopter type, which could be tilted by a servo motor [29]. They controlled the attitude of the vehicle using the quadcopter control algorithm and proportional-integral-derivative (PID) controller. Although four rotors are arranged in a planar placement such as a quadcopter, the reinforcement moment is difficult to overcome owing to the separation between the center of mass (C.M) and the center of buoyancy (C.B).

As presented in previous research, a combined helium-filled aerial platform with a tilting rotor system for omnidirectional movement, dexterous flight capabilities, safety, and high flight efficiency has been suggested. However, despite these fully actuated systems, omnidirectional movement and omniorientation control were not completely separated. Consequently, the usability and application of omnidirectional vehicles are limited. In this paper, the pierced in the middle envelope and C.B and C.M match design that is first tried is analyzed in depth. And, owing to a well-organized aerodynamic model and control method, novel independent omniorientational and omnidirectional flight motion that standard blimp or multirotors hard to do was achieved. As a result, the vehicle can move without tilting or perform variable missions in certain tilting angle. We proved the performance of the mechanism and algorithm of the vehicle through diverse demonstrations. Finally, various flight capabilities and usabilities of 6 DoF under manual control are presented.

The remainder of this paper is organized as follows: Section II describes the design of the vehicle, dynamic model, and control methods. Section III describes flight performance such as omniorientational and omnidirectional motion of the designed vehicle and presents various application cases. Finally, Section IV presents the conclusions and future work.

II. SYSTEM DESIGN

In this section, detail of design, modeling and control algorithm of the platform that realizing omniorientational movement is described.

A. HARDWARE DESIGN

The hull design is a symmetrical torus-type with a hole through the center. The four rotors were symmetrically aligned around the planar hull, as shown in Fig. 1. The height of the hull, which is made of thin PVC material, is 800mm, and the outer and inner diameters are 2200mm and 160mm, respectively. It is very resilient and inflates up to 1000mm in height based on the amount of helium added, and the buoyancy is 2800 g. The weight of the hull is approximately 2000 g with a density of 0.189 kg/m^2. By excluding the weight of the control equipment from the buoyancy, a payload of approximately 100 g is obtained, and it is lifted by a four rotor thrust. Owing to the symmetrical hull shape, the C.B is centered, as shown in Fig. 1. Four pairs of tiltable actuators comprised a 5-inch brushless DC motor (BLDC) and a servo motor. The servo can turn 180°(*e.g.*, ±90°) around each axis and is arranged parallel to each body axis, which is coincident with the C.B, as shown in Fig. 2. Flight-aid electric parts (e.g., flight controller (FC), lithium polymer (LiPo) battery,

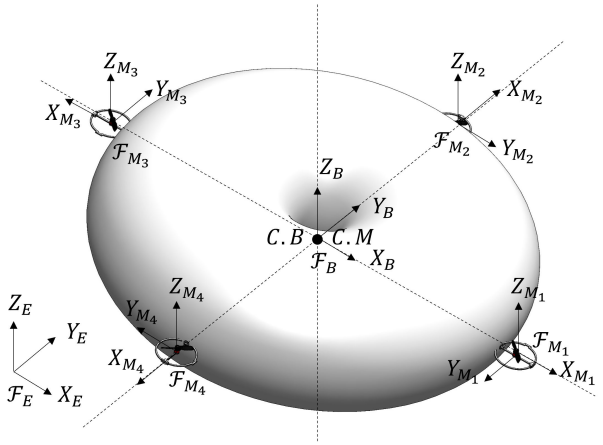

FIGURE 1. Schematic description and reference frames of the blimp.

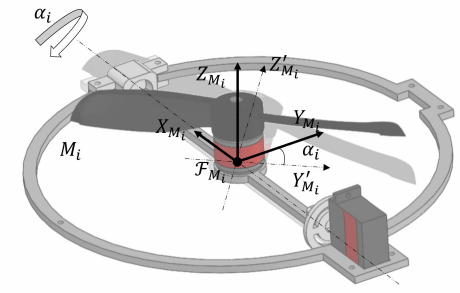

FIGURE 2. Schematic description and reference frames of the tilting actuators.

TABLE 1. Component parts of the vehicle.

Component	Quantity	Weight (g)	Product name
Hull	1	2000	PVC
BLDC motor	4	21	Xnova 1306– 2300 KV
Propeller	4	6	APC 5 inch
ESC	4	10	dys Xs 20A
Servo motor	4	25	md85mg
RC receiver	1	13	Maxima 6
Flight controller	1	23	Self-made
BEC	1	10	BEC 5 V 2 A
Battery	1	200	PT1500 mAh 3-cell
Power distributor	1	10	4 way matek hub
Wire	·	86	·
Frame	·	50	PLA

remote control (RC) receiver, four electric speed controllers (ESCs), and a power distributor) are located in the center of the hull, and the weights of each part are listed in Table. 1. As there is no existing model for FC, it is manufactured using the ATMEGA 2560 chip. ESCs were converted to rotate the BLDC bidirectionally.

B. MODELING

The frame $\mathcal{F}_E : \{X_E Y_E Z_E\}$ is an Earth inertial frame that is fixed on the ground, and the Z_E axis points upward. In addition, the frame $\mathcal{F}_B : \{X_B Y_B Z_B\}$ is a body-fixed frame located at the origin of the C.B of the hull, which coincides with the Center of Volume ($C.V$). Furthermore, the frame $\mathcal{F}_{M_i} : \{X_{M_i} Y_{M_i} Z_{M_i}\}$, where $i = 1...4$, is associated with the center of the i-th tiltable actuator. In addition, each coordinate frame rotates the α_i angle around the X_{M_i} axes with respect to the body frame. Generally, the C.M of the normal quadcopter is designed to be coplanar with the four propellers and the $C.M$ is equal to the center of gravity ($C.G$). In our case, we designed the heavy electric parts to be located in the center of the hole and coplanar with four tiltable actuators. Accordingly, the C.G (i.e., C.M) coincides with the C.B, as shown in Fig. 1.

${}^B\mathbf{R}_E \in SO(3)$ ($Z-Y-X$ Euler angle model in the special orthogonal group) represents the transformation matrix of the Earth inertial frame $\mathcal{F}_E$ to the $C.M$ frame $\mathcal{F}_B$.

$$ {}^B\mathbf{R}_E = \begin{bmatrix} c\psi c\theta & c\psi s\phi s\theta - c\phi s\psi & s\phi s\psi + c\phi c\psi s\theta \\ c\theta s\psi & c\phi c\psi + s\phi s\psi s\theta & c\phi s\psi s\theta - c\psi s\phi \\ -s\theta & c\theta s\phi & c\phi c\theta \end{bmatrix} \quad (1) $$

where $c(\cdot)$ and $s(\cdot)$ are the shorthand forms of cosine and sine, respectively.

The position and orientation of the vehicle according to $\mathcal{F}_E$ are expressed as follows:

$$ \xi^E = \left[(\xi_p^E)^T \ (\xi_o^E)^T \right]^T = \left[x^E \ y^E \ z^E \ \phi \ \theta \ \psi \right]^T \quad (2) $$

where ϕ, θ, and ψ denote the roll, pitch, and yaw Euler angles, respectively. The linear and angular velocities of the vehicle according to $\mathcal{F}_B$ are denoted as follows:

$$ \nu^B = \left[(\mathbf{v}^B)^T \ (\Omega^B)^T \right]^T = \left[v_x^B \ v_y^B \ v_z^B \ \omega_x^B \ \omega_y^B \ \omega_z^B \right]^T \quad (3) $$

From [8], the vehicle kinematic equations can be described as follows:

$$ \dot{\xi} = \mathbf{J}\nu^B $$

or

$$ \begin{bmatrix} \dot{\xi}_p^E \\ \dot{\xi}_o^E \end{bmatrix} = \begin{bmatrix} {}^B\mathbf{R}_E & \mathbf{0}_{3\times3} \\ \mathbf{0}_{3\times3} & {}^B\mathbf{S}_E \end{bmatrix} \begin{bmatrix} \nu^B \\ \Omega^B \end{bmatrix} \quad (4) $$

where

$$ {}^B\mathbf{S}_E = \begin{bmatrix} 1 & s\phi s\theta/c\theta & c\phi s\theta/c\theta \\ 0 & c\phi & -s\phi \\ 0 & s\phi/c\theta & c\phi/c\theta \end{bmatrix} \quad (5) $$

The configurations of the vehicle are described by the position and orientation (ξ_P^W and ξ_O^W) with linear velocity and angular velocity, and by the four tilt angles of the actuators α_i.

The rigid body dynamic motion of the vehicle can be described by the Newton-Euler equations of motion for associating the acceleration with forces and moments. However, unlike the usual quadrotor dynamic model, the added-inertia effects must be considered for modeling. Because the dynamics of the helium-filled vehicle is similar to that of an underwater or submerged one, the 6 DoF nonlinear dynamic equations of the blimp defined in $\mathcal{F}_B$ are described as follows [31]:

$$ \mathbf{M}\dot{\nu}^B + \mathbf{C}(\nu)^B\nu^B + \mathbf{D}(\nu)^B\nu^B + \mathbf{g}(\xi)^E = \tau^B \quad (6) $$

where the terms are defined as follows:

1) $\mathbf{M}$: the vehicle and added-inertia matrix terms
2) $\mathbf{C}(\nu)^B$: the matrix of the Coriolis and centripetal terms
3) $\mathbf{D}(\nu)^B$: the damping matrix terms
4) $\mathbf{g}(\xi)^W$: the restoring forces and moments matrix terms
5) τ^B: the control inputs terms

The detailed derivations are provided in the following subsections.

1) INERTIA MATRIX

The mass and inertia matrix of the vehicle is defined as follows [31]:

$$\mathbf{M}_B = \begin{bmatrix} m\mathbf{I}_{3\times3} & -m(\mathbf{r}_G^b)^\times \\ m(\mathbf{r}_G^b)^\times & \mathbf{J}_B \end{bmatrix} \tag{7}$$

where m is the mass of the vehicle; $\mathbf{I}$ and $\mathbf{J}_B$ are the 3×3 identity matrix and the inertia matrix of the vehicle with respect to $C.M$, respectively. $(\cdot)^\times$ is a skew-symmetric matrix operator and $\mathbf{r}_G^b$ is the coordinate of the C.G in frame C.B. Owing to coincidence of C.B and C.M, this term equals zero as in the usual quadcopter.

Under the assumption that the vehicle flies slowly and has a three-axis symmetric design, the added-mass $\mathbf{A}_m$ and added-inertia matrix $\mathbf{A}_J$ of the vehicle and the diagonal expression can be described as follows:

$$\begin{aligned} \mathbf{M}_{added} &= \begin{bmatrix} \mathbf{A}_m & \mathbf{0}_{3\times3} \\ \mathbf{0}_{3\times3} & \mathbf{A}_J \end{bmatrix} \\ &= diag(\begin{bmatrix} m_{A_x} & m_{A_y} & m_{A_z} & J_{A_x} & J_{A_y} & J_{A_z} \end{bmatrix}^T) \end{aligned} \tag{8}$$

Thus, the inertia matrix of the vehicle can be described as:

$$\begin{aligned} \mathbf{M} &= \mathbf{M}_B + \mathbf{M}_{added} \\ &= diag(\begin{bmatrix} m'_x & m'_y & m'_z & J'_x & J'_y & J'_z \end{bmatrix}^T) \end{aligned} \tag{9}$$

where the added-mass and added-inertia terms are included.

2) CORIOLIS AND CENTRIPETAL EFFECTS

Owing to the vehicle rotation motion, the Coriolis and centripetal effects are applied to the filled gas in the hull. Based on an existing derivation [31], the Coriolis and centripetal matrices are expressed as follows:

$$\mathbf{C}(\nu^B) = \begin{bmatrix} \mathbf{0}_{3\times3} & -(\mathbf{M}_{11}\mathbf{v}^B + \mathbf{M}_{12}\Omega^B)^\times \\ -(\mathbf{M}_{11}\mathbf{v}^B + \mathbf{M}_{12}\Omega^B)^\times & (\mathbf{M}_{21}\mathbf{v}^B + \mathbf{M}_{22}\Omega^B)^\times \end{bmatrix} \tag{10}$$

where $\mathbf{M}_{ij}(i, j = 1, 2)$ are four 3×3 submatrices of inertia matrix M.

3) DAMPING FORCES AND MOMENTS

Owing to the wide surface of the hull, the friction induced by the viscous effects of the surrounding air is negligible and causes damping forces and moments on the vehicle. The drag force is proportional to the velocity of the vehicle for laminar flow and proportional to the square of the velocity for turbulent flow, as shown in the following equation:

$$\mathbf{F}_D = -\frac{1}{2}\rho C_{d_{v_{(\cdot)}}} A_{(\cdot)}(\mathbf{v}^B)^2 = C'_{v_{(\cdot)}}(\mathbf{v}^B)^2_{(\cdot)} \tag{11}$$

where ρ is the density of the air, $C_{d_{v_{(\cdot)}}}$ and $A_{(\cdot)}$, respectively, is the linear drag coefficient and area of each axis of the hull. In addition, the aerodynamic drag moment $\mathbf{M}_D$ is obtained from the derivation in [31]:

$$\mathbf{M}_D = -\frac{1}{2}\rho C_{d_{\omega_{(\cdot)}}} r^5(\Omega^B)^2 = C'_{\omega_{(\cdot)}}(\Omega^B)^2 \tag{12}$$

where r is the diameter of the hull and $C_{d_{\omega_{(\cdot)}}}$ is the rotational drag coefficient of the hull.

As the vehicle moves slowly, the terms higher than the second order (i.e., turbulent flow terms) can be disregarded. Thus, the damping terms are derived as follows:

$$\begin{aligned} &\mathbf{D}(\nu^B)\nu^B \\ &= -diag\begin{bmatrix} C'_{v_x}v_x^2 & C'_{v_y}v_y^2 & C'_{v_z}v_z^2 & C'_{\Omega_x}\Omega_x^2 & C'_{\Omega_y}\Omega_y^2 & C'_{\Omega_z}\Omega_z^2 \end{bmatrix} \end{aligned} \tag{13}$$

4) RESTORING FORCES AND MOMENTS

In a blimp, the $C.G$ to $C.B$ distance determines static stability. Both the buoyancy force F_B act on the $C.B$, and the gravity force F_G acts on the $C.G$. However, by setting $C.G$ equal to $C.B$, the resultant force of buoyancy and gravity is applied at the same point, indicating that the restoring force is not applied. Thus, the restoring force and moments can be neglected. As the restoring force is minimized, the platform will be sensitive to the disturbance like wind. This static instability will be stabilized by maximized moment came from four rotors like an usual multirotors. A stabilization test from disturbance will be dealt at Section III.

5) CONTROL INPUTS

The control inputs τ^G are derived from the propulsive forces of the four propellers and torque moments from the tilting control of the four propellers. As it is designed for a slow flight speed, the inertial effects from the tilting propellers and motor torques can be neglected. Consequently, the inputs depend only on the motor outputs and the mixing control of the tilting mechanism as follows:

$$\tau^B = \begin{bmatrix} \mathbf{F}(\alpha) & \tau(\alpha) \end{bmatrix}^T = \begin{bmatrix} F_x & F_y & F_z & \tau_x & \tau_y & \tau_z \end{bmatrix}^T \tag{14}$$

The thrust generated by a rotor is modeled according to momentum theory, and its lumped model is as follows:

$$\begin{aligned} F_{(\cdot)} &= K_f \rho A_r r_r \omega_{(\cdot)}^2 \\ &= k_f \omega_{(\cdot)}^2 \end{aligned} \tag{15}$$

where K_f is the thrust coefficient, A_r is the rotor disk area, r_r is the radius of the rotor, $\omega_{(\cdot)}$ is the angular velocity of the rotor, and k_f is the lumped coefficient of the thrust model. The *sin* term of the thrust is used to indicate planar movement, and the *cos* term of thrust is used for altitude control. The

total control forces with each tilting angle $\alpha_{(\cdot)}$ are described as follows:

$$\begin{aligned}\mathbf{F}(\alpha) &= (\begin{bmatrix}F_x & F_y & F_z\end{bmatrix})^T \\ &= \begin{bmatrix} 0 & k_f sin\alpha_2 & 0 & k_f sin\alpha_4 \\ k_f sin\alpha_1 & 0 & k_f sin\alpha_3 & 0 \\ k_f cos\alpha_1 & k_f cos\alpha_2 & k_f cos\alpha_3 & k_f cos\alpha_4 \end{bmatrix} \begin{bmatrix} \omega_1^2 \\ \omega_2^2 \\ \omega_3^2 \\ \omega_4^2 \end{bmatrix}\end{aligned} \tag{16}$$

In the case of moment, the reactive torque of the servo is too small compared to the inertia of the aircraft. In addition, the propeller torque is ignored because it is negligible compared to the torque from the thrust. Therefore, the moment caused by the rotor thrust is modeled as follows:

$$\tau_{(\cdot)} = Lk_f\omega_{(\cdot)}^2 \tag{17}$$

The control moments with tilting angle $\alpha_{(\cdot)}$ are described as follows:

$$\begin{aligned}\tau(\alpha) &= (\begin{bmatrix}\tau_x & \tau_y & \tau_z\end{bmatrix})^T \\ &= \begin{bmatrix} 0 & -Lk_f cos\alpha_2 & 0 & Lk_f cos\alpha_4 \\ -Lk_f cos\alpha_1 & 0 & Lk_f cos\alpha_3 & 0 \\ -Lk_f sin\alpha_1 & Lk_f sin\alpha_2 & -Lk_f sin\alpha_3 & Lk_f sin\alpha_4 \end{bmatrix} \\ &\quad \times \begin{bmatrix} \omega_1^2 \\ \omega_2^2 \\ \omega_3^2 \\ \omega_4^2 \end{bmatrix}\end{aligned} \tag{18}$$

Owing to the tilting angle α_i, this system has an advantage in that the force vector can be adjusted in any orientation during flight. Although the control input matrix size is 4×6, as in the usual quadcopter, the system can produce the desired force in all three axes of $\mathscr{F}_E$ in any orientation by tilting the rotors (e.g., an insufficient rank of configurations can be adjusted with α_i). This means the translation and rotation motions of the vehicle can be independently controlled with force and torque inputs respectively. The novel independent position and orientation control algorithm for this system is proposed in the next section.

C. CONTROL DESIGN

The object of the control algorithm for the vehicle is independent stable omniorientation and omnidirection control, which implies facilitating both omnidirectional flight movements maintaining any attitude, as well as horizontal flight movements similar to conventional drones. We used the torque inputs $\tau(\alpha)$ for attitude control and force inputs $\mathbf{F}(\alpha)$ for position control independently.

As the C.B and C.M of the vehicle coincide, the reinforcement force that hinders the stabilization of the usual blimp vanishes. Owing to this characteristic, the inertia of the vehicle is simplified and low. Thus, the dynamic motion is similar to that of a common quadcopter. However, unlike most used cascade control structure in quadcopter [19], our proposed attitude control is based on a single PID control. It is sufficient for tracking the target orientation of the vehicle by controlling the angular speed of each motor. The Euler angle error is defined as the difference between the desired and current angle of the vehicle $\mathbf{s}_e = \mathbf{s}_d - \mathbf{s}_c$, where $\mathbf{s}$ can be θ, ψ, and ϕ. Than the attitude control method is as follows:

$$\tau_{(\cdot)} = \kappa_1(K_P^I\dot{\mathbf{s}}_e + K_I^I\int\dot{\mathbf{s}}_e + K_D^I\ddot{\mathbf{s}}_e) \tag{19}$$

where K_P^I, K_I^I, and K_D^I are the gains of the PID terms.

As shown in Fig. 1, Y_B axis angle (roll) is controlled by $\mathscr{F}_{M_2}$ and $\mathscr{F}_{M_4}$ motors. Similarly, the X_B axis angle (pitch) is controlled by $\mathscr{F}_{M_1}$ and $\mathscr{F}_{M_3}$ motors. And the Z_B axis angle (yaw) is controlled by simultaneously tilting the four motors. These axes control allocation is applied not only in level hovering but also in vertical or flip conditions. Owing to the symmetrical design of the vehicle, 3 DoF rotational motions (roll, pitch, and yaw) are conducted between each control axis and motor pair, as shown in Fig. 3. By maintaining each control axis, X_E and Y_E translational motion are achieved by tilting the two Y_B-axis and X_B-axis motors, respectively. These control allocations do not change during vertical and flip motion.

III. FLIGHT PERFORMANCE

Various flight experiments were performed to validate the performance of the vehicle. This section discusses, level stabilization flight, vertical and inverted flight, omniorientation flight, and omnidirection flight tests, along with application cases. Each control target is determined with manual control by a pilot, and orientation and position data are measured by the IMU and external indoor GPS system, respectively.

A. LEVEL STABILIZATION FLIGHT

Using a single PID controller for stable level flight, the roll, pitch, and yaw angles of the vehicle are controlled, and the test results are presented in Fig. 4. The roll target ($-3°$), pitch target ($-5°$), and yaw target ($-10°$) were set, and $K_P^I = 0.6$, $K_I^I = 0.1$, and $K_D^I = 0.5$ were also applied. But in the case of yaw control, $K_P^I = 0.4$ is applied because of the sensitivity of servo control. We found these parameter from lots of trial. The offset of the roll and pitch from zero angle originate from the initial mount error of the FC. It maintains each target angle with an error of $\pm 1°$ during the front part of a 300 s flight, as shown in Fig. 4. Despite of external disturbances are applied in each axis (roll, pitch, and yaw), the vehicle showed fast recovery during the back part of a 300 s flight. The adopted single PID controller was sufficient for stable attitude control and omniorientation control. The vehicle overcomed pendulum motion that standard blimp experience [9] and shows more fast and stable level flight results.

B. VERTICAL AND INVERTED FLIGHT

Each target angle tracking control was tested during the vehicle transition from the level position to the vertical and inverted positions. Fig. 5 presents the transition results. The transition was executed by rotating the roll angle (X_B) and the rotation speed was $0.0523 rad/s$. During the flip transition, tracking loss occurred at the vertical position frequently

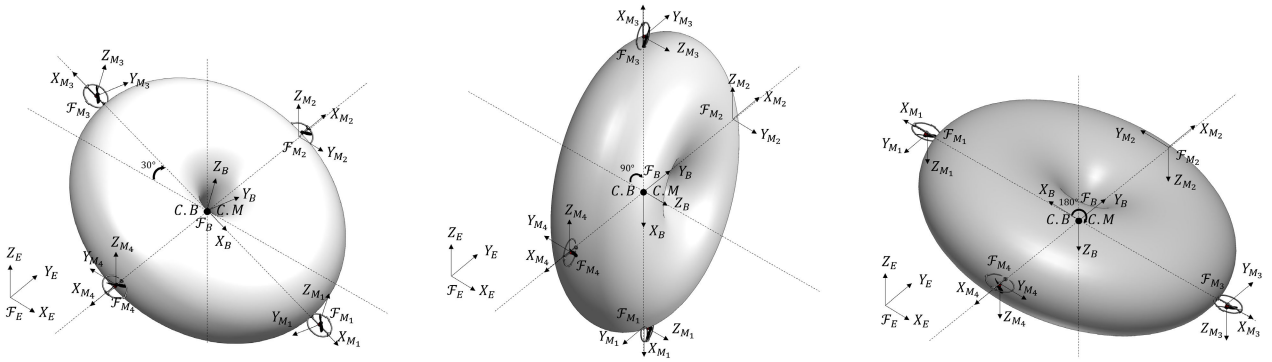

(a) 30° (b) 90° (c) 180°

FIGURE 3. Schematic description and reference frames of the tiltable actuators.

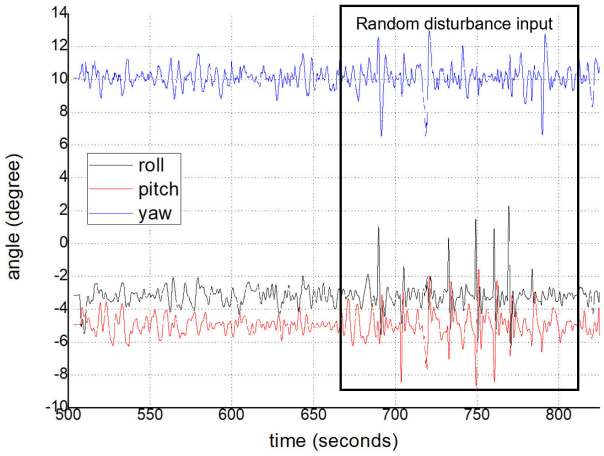

FIGURE 4. Attitude stabilization control flight result.

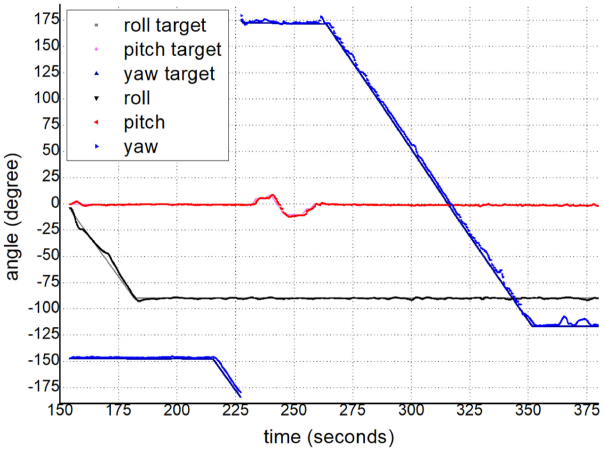

(a) vertical transition

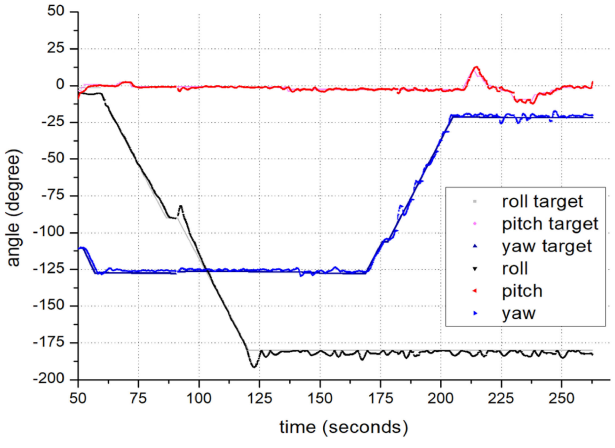

(b) inverted transition

FIGURE 5. Vertical and inverted position control flight result.

because of the flipping of two motor coordinates, ($\mathcal{F}_{M_2}$ and $\mathcal{F}_{M_4}$), as shown in Fig. 3(b) and 3(c). This transition is an essential process owing to the limited rotation angle of the servos. After each transition, the vehicle showed stable pitch and yaw control, as shown in Fig. 5(a) and 5(b). It followed the target angle of manual input by the pilot, and the yaw rotation speed was $0.0447 rad/s$. The rotation speed of each axis can be adjusted as required. Snapshots of the level to inverted position transition and pitch and yaw rotation in each position are presented in Fig. 6. The pitch axis control (Y_B) depends on the Y_E translation movement showing lateral floating during pitch control, as shown in Fig. 6(c) and 6(e).

C. OMNIORIENTATION FLIGHT

In addition to certain angle transitions, such as vertical and inverted positions, an omniorientational control test manual input by pilot was performed. The pilot maneuvered the roll, pitch, and yaw angles randomly, and the vehicle followed it, as shown in Fig. 7. During the rotation of the roll angle of the vehicle (X_B) before the inverted position, two motors ($\mathcal{F}_{M_2}$ and $\mathcal{F}_{M_4}$), which are located on the Y_B axis, are parallel to the Z_E axis to maintain the altitude, as shown in Fig. 3(b). After flipping upside down, all motors ($\mathcal{F}_{M_1}$, $\mathcal{F}_{M_2}$, $\mathcal{F}_{M_3}$, and $\mathcal{F}_{M_4}$) revert to the initial position and rotate in anti-direction, as shown in Fig. 3(c). This experiment shows the vehicle capabilities that not feasible to standard multirotors but easy

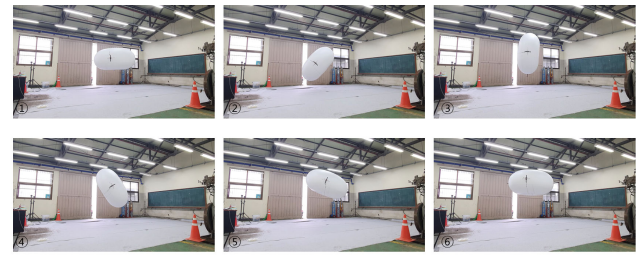

(a) roll transition from level to inverted position

(b) yaw rotation in vertical position

(c) pitch rotation in vertical position

(d) yaw rotation in inverted position

(e) pitch rotation in inverted position

FIGURE 6. Transition from level to inverted position control flight.

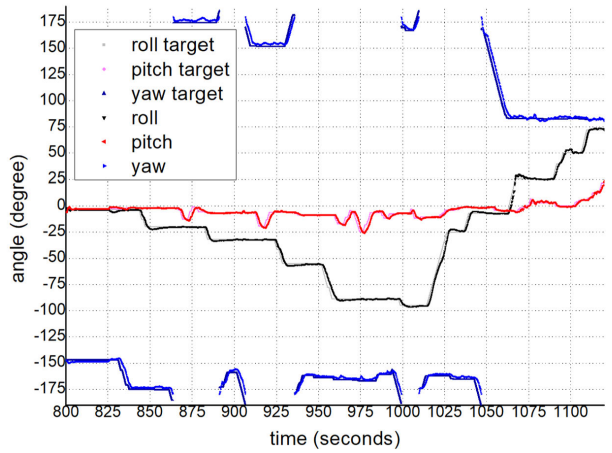

FIGURE 7. Omniorientation control flight result.

to this platform. It can be performed with simple mechanism, lightweight system, and easy-to-repair design [24].

D. OMNIDIRECTION FLIGHT

Omnidirectional flight with manual input control by pilot during tilted position is performed. Fig. 8 presents the

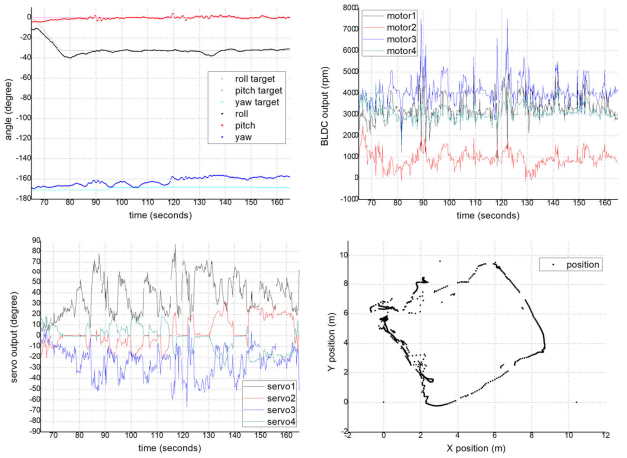

(a) flight data during 32° rolling

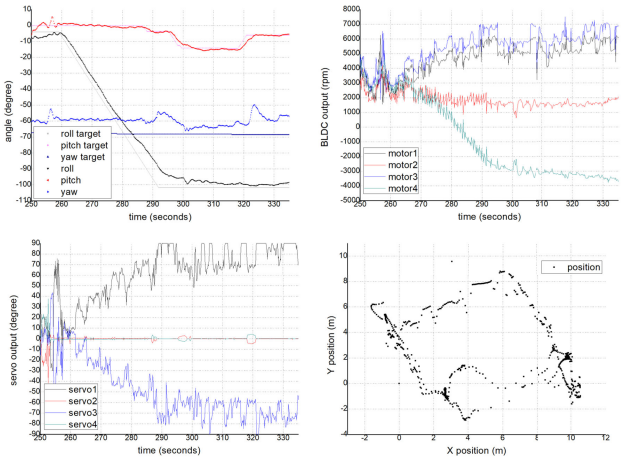

(b) flight data during 101° rolling

FIGURE 8. Orientation, motor, servo, and position data during tilted position.

motor, servo and position data. During two tilted orientations (32° and 101°) flight, four servo and four BLDC motors were controlled using the designed control method. As the vehicle climbed vertically, two motors ($\mathscr{F}_{M_2}$ and $\mathscr{F}_{M_4}$) rotate faster to maintain the altitude, and the tilting angle of each servo increases in the opposite direction. In addition, the other two motors ($\mathscr{F}_{M_1}$ and $\mathscr{F}_{M_3}$) keep rotating to follow the target roll angle, and the tilting angle of each servo maintains the initial position. By retaining the target orientation, lateral translation is maneuvered by the pilot, and the position data are measured by the inner GPS system. The vehicle was stably followed along the lateral wall of the building. It followed four routes by controlling the tilting angle of each axis servo without turning the yaw angle of the vehicle.

E. APPLICATIONS

Several application cases are tested wherein general quadcopters find it difficult to show novel specifications of this vehicle. As the design of the vehicle is similar to a donut, passing a narrow space (e.g., door) with level position flight

FIGURE 9. Snapshots of narrow door passing of the vehicle.

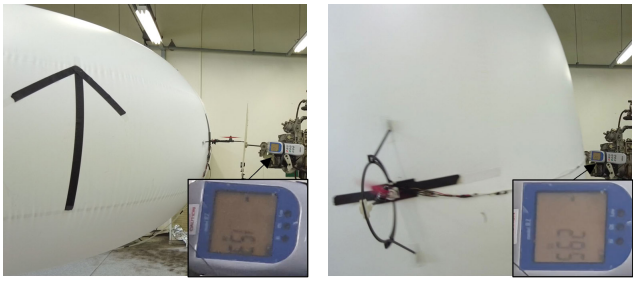

(a) contact force in level position (b) contact force in vertical position

FIGURE 10. Omnidirectional contact force measurement test.

is difficult. The omniorientation control of the vehicle makes it possible for the vehicle to pass through the narrow space, as shown in Fig. 9, by transitioning to the vertical position. A fairly stable interaction with a wall or board without changing the vehicle orientation is useful for wall-touching work. Lateral and downward contact force measurements were performed to prove this application, as in [21]. In our case, to prove the omnidirectional contact force with orientation control, the lateral contact force was measured with the lateral and vertical positions, as shown in Fig. 10. The pushed force was measured using a push-pull gauge tool. A force of 1.53 N was measured in the lateral position, and a force of 2.95 N was measured in the vertical position, as shown in Fig. 10(a) and 10(b), respectively. The lateral force in the vertical position is larger because the two motors in $\mathcal{F}_B$ coordinates can push parallel to the direction the vehicle flies in.

IV. CONCLUSION

In this study, we developed a novel unmanned blimp design and control algorithm for independent omnidirection and omniorientation controllable flight. It is a helium-filled torus-type blimp comprising four pairs of tiltable actuators and a PID controller that ensures safety, long time flight, and omnidirectional motion. Owing to the model-based free-reinforcement design, the vehicle showed stable rotation and target angle tracking. The symmetric design of the vehicle made it possible to follow all orientations with each axis rotation. In addition, it performed stable and safe translational motion alongside the pilot maneuvers owing to its light weight and independent control allocation. Buoyancy-aided energy reduction has enabled the development of an efficient drone and simple control for diverse applications. Diverse performance validation tests were performed, and the results proved stable flight and applicability. Expanded maneuverability provided extraordinary applications, such as narrow space passing and physical interaction with the omnidirectional surface, thereby overcoming the limitations of the normal quadcopter. Also, as the vehicle can flip, both of surface can be used for advertisement by printing a pictures. Pick and place [12], torque generation [28], following people safely with vision camera [31], and drone surveillance [32] are potential usability of this platform. In addition, this symmetrical coincidence of the C.B and the C.G design with the surrounding four tiltable actuators can be applied to other shapes of the envelope. Making large size of the hull for getting sufficient buoyancy makes lateral damping force large too. And, versatile maneuverability decreases lateral force of the vehicle. Slow flight speed caused by these factors and it also hard to overcome wind disturbance. Owing to this limitation, this vehicle is suitable to fly indoor space.

In future work, a more elaborate control algorithm for 6-axes-independent rotation and translation motion and disturbance compensation-based design for outdoor flight would be researched. And, optimal PID control research about diverse size and weight is needed. Furthermore, omnidirectional aerial records with center-mounted camera and printing advertisements on both sides of the surface are expected applications.

REFERENCES

[1] V. Kumar and N. Michael, "Opportunities and challenges with autonomous micro aerial vehicles," *Int. J. Robot. Res.*, vol. 31, no. 11, pp. 1279–1291, 2012.
[2] D. Floreano and R. J. Wood, "Science, technology and the future of small autonomous drones," *Nature*, vol. 521, no. 7553, pp. 460–466, 2015.
[3] R. Mahony, V. Kumar, and P. Corke, "Multirotor aerial vehicles: Modeling, estimation, and control of quadrotor," *IEEE Robot. Autom. Mag.*, vol. 19, no. 3, pp. 20–32, Sep. 2012.
[4] H. Yang, Y. Lee, S.-Y. Jeon, and D. Lee, "Multi-rotor drone tutorial: Systems, mechanics, control and state estimation," *Intell. Service Robot.*, vol. 10, no. 2, pp. 79–93, Apr. 2017.
[5] A. V. Asares, P. S. Ko, J. S. Minlay, B. R. Sarmiento, and A. Chua, "Design of an unmanned aerial vehicle blimp for indoor applications," *Int. J. Mech. Eng. Robot. Res.*, vol. 8, no. 1, pp. 157–161, 2018.
[6] S. H. Song and H. R. Choi, "A novel tandem-type soft unmanned aerial vehicle: Mechanism design, performance validation and implementation," in *Proc. 18th Int. Conf. Ubiquitous Robots (UR)*, Jul. 2021, pp. 363–370.
[7] C. Wan, N. Kingry, and R. Dai, "Design and autonomous control of a solar-power blimp," in *Proc. AIAA Guid., Navigat., Control Conf.*, Jan. 2018, p. 1588.
[8] Y. Wang, G. Zheng, D. Efimov, and W. Perruquetti, "Disturbance compensation based control for an indoor blimp robot," in *Proc. Int. Conf. Robot. Autom. (ICRA)*, May 2019, pp. 2040–2046, doi: 10.1109/ICRA.2019.8793535.
[9] H. Suefuku, T. Hirayama, Y. Hirakawa, and T. Takayama, "Torus-type airship aiming at high airworthiness quality," in *Proc. Interface Cong. Aero. Sci.*, 2010, pp. 1–10.
[10] S. H. Song, G. Y. Yeon, H. W. Shon, and H. R. Choi, "Design and control of soft unmanned aerial vehicle 'S-CLOUD,'" *IEEE/ASME Trans. Mechatronics*, vol. 26, no. 1, pp. 267–275, Feb. 2021.
[11] Q. Tao, J. Wang, Z. Xu, T. X. Lin, Y. Yuan, and F. Zhang, "Swing-reducing flight control system for an underactuated indoor miniature autonomous blimp," *IEEE/ASME Trans. Mechatronics*, vol. 26, no. 4, pp. 1895–1904, Aug. 2021, doi: 10.1109/TMECH.2021.3073966.
[12] *FreeMotionHandling*. Accessed: 2021. [Online]. Available: https://www.festo.com/group/en/cms/11957.htm

[13] W. Yamada, H. Manabe, and D. Ikeda, "ZeRONE: Safety drone with blade-free propulsion," in *Proc. CHI Conf. Hum. Factors Comput. Syst.*, May 2019, pp. 1–8.
[14] Y. H. Pheh, S. K. H. Win, and S. Foong, "SpICED: Design and control of a safe spherical blimp using coandă effect," in *Proc. IEEE/ASME Int. Conf. Adv. Intell. Mechatronics (AIM)*, Jul. 2021, pp. 270–277.
[15] D. St-Onge, P.-Y. Brèches, I. Sharf, N. Reeves, I. Rekleitis, P. Abouzakhm, Y. Girdhar, A. Harmat, G. Dudek, and P. Giguère, "Control, localization and human interaction with an autonomous lighter-than-air performer," *Robot. Auto. Syst.*, vol. 88, pp. 165–186, Feb. 2017.
[16] S. Ghassemi and D. Hong, "Feasibility study of a novel robotic system BALLU: Buoyancy assisted lightweight legged unit," in *Proc. IEEE-RAS 16th Int. Conf. Humanoid Robots (Humanoids)*, Nov. 2016, p. 144.
[17] R. Rashad, J. Goerres, R. Aarts, J. B. C. Engelen, and S. Stramigioli, "Fully actuated multirotor UAVs," *IEEE Robot. Atuto. Mag.*, vol. 27, no. 3, pp. 97–107, Feb. 2020.
[18] G. Heredia, A. E. Jimenez-Cano, I. Sanchez, D. Llorente, V. Vega, J. Braga, J. A. Acosta, and A. Ollero, "Control of a multirotor outdoor aerial manipulator," in *Proc. IEEE/RSJ Int. Conf. Intell. Robots Syst.*, Sep. 2014, pp. 3417–3422.
[19] Y. Qin, W. Xu, A. Lee, and F. Zhang, "Gemini: A compact yet efficient bi-copter UAV for indoor applications," *IEEE Robot. Autom. Lett.*, vol. 5, no. 2, pp. 3213–3220, Apr. 2020, doi: 10.1109/LRA.2020.2974718.
[20] M. Ryll, H. H. Bulthoff, and P. R. Giordano, "A novel overactuated quadrotor unmanned aerial vehicle: Modeling, control, and experimental validation," *IEEE Trans. Control Syst. Technol.*, vol. 23, no. 2, pp. 540–556, Mar. 2015, doi: 10.1109/TCST.2014.2330999.
[21] M. Odelga, P. Stegagno, and H. H. Bulthoff, "A fully actuated quadrotor UAV with a propeller tilting mechanism: Modeling and control," in *Proc. IEEE Int. Conf. Adv. Intell. Mechatronics (AIM)*, Jul. 2016, pp. 306–311.
[22] A. Junaid, A. Sanchez, J. Bosch, N. Vitzilaios, and Y. Zweiri, "Design and implementation of a dual-axis tilting quadcopter," *Robotics*, vol. 7, no. 4, p. 65, Oct. 2018.
[23] M. Kamel, S. Verling, O. Elkhatib, C. Sprecher, P. Wulkop, Z. Taylor, R. Siegwart, and I. Gilitschenski, "The voliro omniorientational hexacopter: An agile and maneuverable tiltable-rotor aerial vehicle," *IEEE Robot. Autom. Mag.*, vol. 25, no. 4, pp. 34–44, Dec. 2018, doi: 10.1109/MRA.2018.2866758.
[24] S. Park, J. Lee, J. Ahn, M. Kim, J. Her, G.-H. Yang, and D. Lee, "ODAR: Aerial manipulation platform enabling omnidirectional wrench generation," *IEEE/ASME Trans. Mechatronics*, vol. 23, no. 4, pp. 1907–1918, Aug. 2018.
[25] B. Li, L. Ma, D. Huang, X. Sun, and T. Hou, "Designing, modeling, and control allocation strategy of a novel omnidirectional aerial robot," in *Proc. IEEE Conf. Control Technol. Appl. (CCTA)*, Aug. 2019, pp. 762–767.
[26] A. Franchi, R. Carli, D. Bicego, and M. Ryll, "Full-pose tracking control for aerial robotic systems with laterally bounded input force," *IEEE Trans. Robot.*, vol. 34, no. 2, pp. 534–541, Apr. 2018.
[27] M. Ramp and E. Papadopoulos, "On modeling and control of a holonomic vectoring tricopter," in *Proc. IEEE/RSJ Int. Conf. Intell. Robots Syst. (IROS)*, Sep. 2015, pp. 662–668, doi: 10.1109/IROS.2015.7353443.
[28] M. Burri, L. Gasser, M. Kach, M. Krebs, S. Laube, A. Ledergerber, D. Meier, R. Michaud, L. Mosimann, L. Muri, C. Ruch, A. Schaffner, N. Vuilliomenet, J. Weichart, K. Rudin, S. Leutenegger, J. Alonso-Mora, R. Siegwart, and P. Beardsley, "Design and control of a spherical omnidirectional blimp," in *Proc. IEEE/RSJ Int. Conf. Intell. Robots Syst.*, Nov. 2013, pp. 1873–1879, doi: 10.1109/IROS.2013.6696604.
[29] M. Azizi, M. F. Sedan, and S. M. Harithuddin, "Development of attitude control system for hybrid airship vehicle," *Interface J. Eng. Tech*, vol. 7, no. 4, pp. 99–106, Oct. 2018.
[30] T. I. Fossen, *Handbook of Marine Craft Hydrodynamics and Motion Control*. Hoboken, NJ, USA: Wiley, 2011.
[31] B. Jeon, Y. Lee, J. Choi, J. Park, and H. J. Kim, "Autonomous aerial dual-target following among obstacles," *IEEE Access*, early access, Oct. 4, 2021, doi: 10.1109/ACCESS.2021.3117314.
[32] S. J. Park, H. T. Kim, S. M. Lee, H. T. Joo, and H. N. Kim, "Survey on anti-drone systems: Components, designs, and challenges," *IEEE Access*, vol. 9, pp. 42635–42650, 2021.

SEUNG HWAN SONG (Student Member, IEEE) received the B.S. degree in mechanical engineering from Sungkyunkwan University, Suwon, Republic of Korea, in 2015, where he is currently pursuing the Ph.D. degree with the School of Mechanical Engineering. He has been with the Robotics Innovatory Laboratory, School of Mechanical Engineering, Sungkyunkwan University, since 2015. His current research interests include coandă effect, drones, robot systems, control, and mechanism.

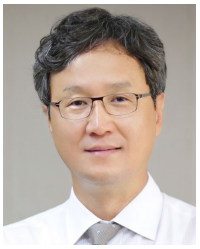

HYOUK RYEOL CHOI (Fellow, IEEE) received the B.S. degree in mechanical engineering from Seoul National University, Seoul, South Korea, the M.S. degree in mechanical engineering from the Korea Advanced Institute of Science and Technology, Daejeon, South Korea, and the Ph.D. degree in mechanical engineering from the Pohang University of Science and Technology, Pohang, South Korea, in 1984, 1986, and 1994, respectively.

From 1986 to 1989, he was an Associate Research Engineer with the IT Research Center, LG Electronics. From 1993 to 1995, he was a Postdoctoral Researcher with Kyoto University, Kyoto, Japan. From 1999 to 2000, he visited the National Institute of Advanced Industrial Science and Technology, Japan, as a JSPS Fellow. From 2008 to 2009, he was a Visiting Professor with the University of Washington, Seattle, USA. Since 1995, he has been a Professor with the School of Mechanical Engineering, Sungkyunkwan University, Suwon, South Korea. His research interests include soft robotics, robotic mechanisms, field applications of robots, dexterous robotic hands, and manipulation.

Prof. Choi was the Founding Co-Chair of the IEEE RAS Technical Committee "Robot Hand, Grasping and Manipulation." He was the General Chair of the 2012 IEEE Conference on Automation Science and Engineering (CASE), Seoul. He was an Associate Editor of IEEE TRANSACTION ON ROBOTICS, the Technical Editor of the IEEE/ASME TRANSACTIONS ON MECHATRONICS, and the Senior Editor of journal of *Intelligent Service Robotics*.